2017 IEEE International Conference on Advanced Intelligent Mechatronics (AIM)
Sheraton Arabella Park Hotel, Munich, Germany, July 3-7, 2017

Fast hybrid position / force control of a parallel kinematic load simulator for 6-DOF Hardware-in-the-Loop axle tests

Andreas Kohlstedt, Phillip Traphöner, Simon Olma, Karl-Peter Jäker and Ansgar Trächtler
Control Engineering and Mechatronics, Heinz Nixdorf Institute, Paderborn University
Fürstenallee 11, 33102 Paderborn, Germany
Email: {andreas.kohlstedt, phillip.traphoener, simon.olma, karl.peter.jaeker, ansgar.traechtler}@hni.uni-paderborn.de

液压六轴

***Abstract*— This contribution presents a hybrid position / force control strategy which is used to operate a hydraulic hexapod in contact with a complex environment. The hexapod serves as an excitation unit in a Hardware-in-the-Loop axle test rig. It is used to reproduce measured or simulated road excitations on the wheel carrier of a MacPherson suspension strut which is rigidly connected to it via a wheel force transducer. The overall test rig system provides a novel method for the development and testing of mechatronic vehicle axles. Following a short introduction and description of the test rig, the modeling and control of the hexapod is presented. Test rig measurements for a square force and position input as well as a sinusoidal force input are provided to evaluate the control performance achieved thus far.**

***Index Terms*— parallel kinematics, load simulator, hybrid position / force control, vehicle axle test rig.**

I. Introduction

Hardware-in-the-Loop (HiL) simulations are widely adopted in the development and validation of electronic control units (ECUs). During a HiL simulation, a specific component of an overall system is tested under laboratory conditions. The device under test, e.g. an ECU, is physically present. All other components of the real-world system which are of relevance to the ECU are replaced by simulations, i.e. numerical models.

HiL simulations are not limited to the situation where the ECU resembles the device under test. In fact, various examples exist where a greater portion of the real-world system has been built up in the laboratory, cf. [1], [2], [3]. When the distinction made in [4] is adopted, the HiL simulation then is no longer conducted at signal level (as in case of the ECU as device under test) but at mechanical level. By shifting the boundary between real and virtual system parts in this way, the system's similarity to its real-world counterpart rises and the outcome of the HiL simulation gains in value. However, by increasing the physically built-up portion of the real-world system, the complexity of the test rig system required for the execution of the corresponding HiL simulation increases. On mechanical level, load machines are necessary to reproduce mechanical loads on the device under test. Depending on the specific situation, the development and operation of these devices during the HiL simulation poses a challenge on its own.

The axle test rig of the Heinz Nixdorf Institute enables the operator to conduct HiL simulations with a physically present axle, see Fig. 1. The test rig provides a novel, sophisticated means for the development of chassis control systems.

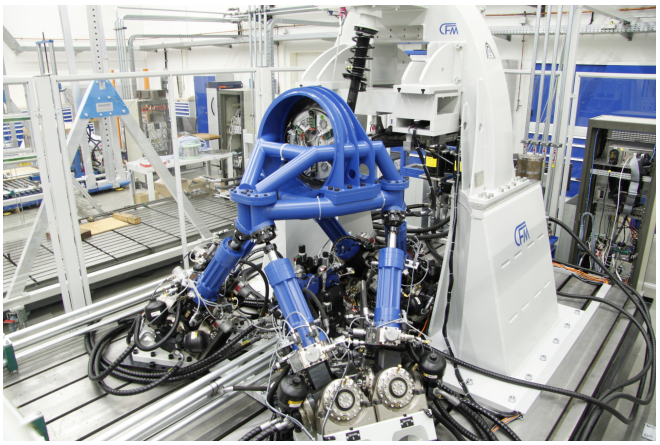

Fig. 1: Test rig for mechatronic axles

The load machine used to simulate road excitations on this particular test rig is a hydraulically actuated hexapod. The end effector of this parallel kinematic machine is attached to six synchronous hydraulic cylinders. It is rigidly connected to a wheel force transducer which in turn is attached to the left wheel carrier of the axle. The axle itself is rigidly mounted to an axle fixture system. When the hydraulic cylinders are appropriately actuated, given mechanical loads on the wheel carrier can be reproduced on the test rig. The mechanical loads can either be computed during simulation runtime, e.g. by means of a detailed environment model, or can originate from recordings of real-world driving maneuvers. An elaborate description of the test rig can be found in [5] while possible HiL simulation scenarios and control strategies are discussed in [6] and [7].

The contribution at hand focuses on the control design for the parallel kinematic load simulator. In particular, force control design is discussed and a detailed assessment of the force control performance is provided.

This article is structured as follows: the next section provides a brief discussion of the state of the art regarding force control of parallel kinematic machines. In Section III, the hexapod model used for control design is described and its equations of motion are derived. These equations are then used in Section IV for the development of the position and force control algorithms of the hexapod. Section V shows

actual measurements obtained on the axle test rig using the presented control approach. The last section concludes the article.

II. State of the art

In robotics, two sets of coordinates to characterize the end effector pose are often referred to. On the one hand, there is the set of so-called joint space coordinates denoted by q subsequently. These coordinates describe the state of each drive, e.g. the stroke or overall length of a linear drive. On the other hand, there are the so-called operational space coordinates referred to by z in the present article. For a robot with six degrees of freedom (DOFs), the vector z usually contains the three Cartesian coordinates of the tool center point (TCP) and a representation of the end effector's rotation, e.g. a set of Euler angles. In most cases, the robot's task is formulated in operational space coordinates.

For parallel mechanisms, the vector of joint space coordinates q can easily be obtained from a given vector of operational space coordinates z by utilizing basic linear algebra. This is the so-called inverse (or indirect) kinematics problem. The opposite operation called forward (or direct) kinematics problem, however, is not explicitly solvable for most mechanisms.

Given these definitions, two basic approaches for the motion control of parallel kinematic mechanisms (as for serial kinematic mechanisms) exist: joint space and Cartesian (or operational / task) space control [8], see Fig. 2.

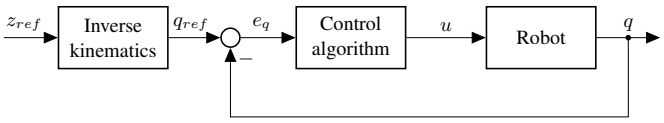

(a) Control in joint space coordinates

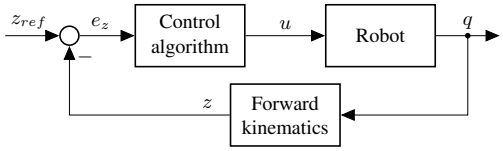

(b) Control in operational space coordinates

Fig. 2: Comparison of joint and operational space control

In Fig. 2, u denotes the physical system input. As the picture indicates, in case of a joint space control approach, a given reference position vector z_{ref} is first transformed to joint space coordinates q_{ref} by means of the inverse kinematics which is then used for the computation of a control algorithm formulated in joint space coordinates.

In contrast, operational space control features a control loop directly in operational space coordinates z. Since z is - in most cases - not directly measured, it has to be computed from given measurements for q by means of the forward kinematics during simulation runtime.

Due to the fact that the solution of the forward kinematics is omitted, joint space control is easier to implement for parallel mechanisms than operational space control. However, operational space control is superior to joint space control for various reasons such as increased speed, stability and accuracy, see [8]. It was chosen for the control of the system at hand.

When a robot interacts with the environment, pure motion control laws are inadequate as they do not account for contact situations. Force control techniques have to be implemented, which can be partitioned in two general strategies: indirect and direct force control.

Indirect force control laws such as compliance control and impedance control do not include an explicit closure of a force control loop. Instead, a desired end effector behavior during contact is realized by means of the control law. A rather new example for an impedance controlled parallel kinematic machine is given by [9]. Simulations prove the functionality of the impedance control law based on a joint space motion controller for an electrohydraulic hexapod. This technique was also presented and evaluated in [7] for a simulation model of the given axle test rig.

Direct force control approaches feature a force control loop. Often, a subordinate controller such as a motion and / or velocity controller is present. One existing direct force control technique is parallel position / force control. While both a position and a force control loop for each direction exist, the force controller is prioritized as it has an integral term in contrast to the position controller. It was used in [10] for a parallel kinematic assembly machine performing the popular peg-in-hole task in various simulations. The approach was adopted in [11] where a vision system was used to determine the current end effector pose z. Simulations for various parallel mechanisms in contact with flat surfaces, including a hexapod, are provided.

An other direct force control approach is hybrid position / force control [12]. This technique basically combines both position and force control algorithms by means of a diagonal selection matrix S. Its entries are either 1 for a force-controlled or 0 for a position-controlled DOF. For instance, hybrid position / force control is used in [13] for a hexapod with linear direct drives. There, the force controller features a subordinate motion control loop in joint space coordinates. Actual measurement results demonstrate its functionality: a desired force level is achieved shortly after contact to a flat surface is made.

To our best knowledge, no examples for force-controlled parallel mechanisms with an operational space control scheme exist which use observer techniques for state estimation. This approach was implemented for the system under consideration. Regarding the specific example, the use of iterative control approaches, e.g. [14], is deliberately avoided. The control results are obtained directly without any iterations, so that the overall system enables HiL simulations to be conducted.

III. System modeling

For control and observer design purposes, the hexapod's end effector platform was modeled as a single rigid body. Fig. 3 shows a schematic of the simplified model.

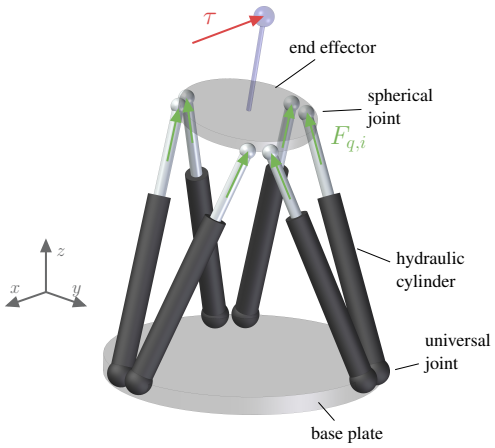

Fig. 3: Simplified hexapod model

Subsequently, the actuators are assumed to provide ideal force inputs. This assumption is valid as the differential pressure controllers of the hydraulic cylinders have a very high bandwidth. For the derivation of the pressure controllers, refer to [15]. The actuator forces are

$$F_q = \begin{bmatrix} F_{q,1} & \dots & F_{q,6} \end{bmatrix}^T = A_{cyl} \cdot \begin{bmatrix} \Delta p_1 & \dots & \Delta p_6 \end{bmatrix}^T$$

where A_{cyl} equals the cylinder piston area. The axle appears in the form of the generalized force vector

$$\tau = \begin{bmatrix} F_x & F_y & F_z & M_x & M_y & M_z \end{bmatrix}^T$$

which contains the forces and torques acting between end effector and wheel carrier. They are directly measured by the wheel force transducer present at the TCP.

The end effector's current pose with respect to an inertial coordinate frame, i.e. the TCP's Cartesian coordinates r_x, r_y and r_z and the end effector's rotation in terms of the Cardan angles α, β and γ, is described by

$$z = \begin{bmatrix} r_x & r_y & r_z & \alpha & \beta & \gamma \end{bmatrix}^T.$$

Given these quantities, the end effector's equations of motion are

$$M(z) \cdot \ddot{z} + C(z, \dot{z}) \cdot \dot{z} + g(z) = J^{-T}(z) \cdot F_q - \tau \qquad (1)$$

where $M(z) \in \mathbb{R}^{6\times6}$ is the pose-dependent inertia matrix, $C(z, \dot{z}) \cdot \dot{z} \in \mathbb{R}^{6\times1}$ is the vector of centrifugal and Coriolis forces, $g(z) \in \mathbb{R}^{6\times1}$ is the vector of gravitational forces and $J(z) \in \mathbb{R}^{6\times6}$ is the manipulator's geometric Jacobian. $J(z)$ can be calculated from

$$J(z) = H(z) \cdot J_A(z)$$

with the system's kinematic matrix

$$H(z) = \frac{\partial v}{\partial \dot{z}}$$

which relates the system's vector of translational and angular velocities v to the time derivative of z and the manipulator's analytical Jacobian

$$J_A(z) = \left(\frac{\partial q}{\partial z} \right)^{-1}. \qquad (2)$$

In (2),

$$q = \begin{bmatrix} q_1 & \dots & q_6 \end{bmatrix}^T$$

is the vector of cylinder lengths which are directly measured on the test rig. It is the system's vector of joint space coordinates while z is its vector of task space coordinates.

IV. Control Strategy

The control approach described subsequently relies on the knowledge of the generalized position vector z and its derivative with respect to time $\dot{z}$ which are not measured on the target system. Instead, they are estimated from the measurements of the cylinder lengths q, the cylinders' differential pressures Δp_i and the contact forces and torques τ. For this purpose, a Kalman filter and a sliding mode observer were designed for the given system [16]. Both simulations and test rig measurements indicate that the sliding mode observer is superior to the Kalman filter in the case at hand. Its design is based on the hierarchical sliding mode observer by Drakunov [17] but was extended to systems with multiple outputs. With the given estimates $\hat{z}$ and $\dot{\hat{z}}$ for z and $\dot{z}$, operational space control algorithms can be implemented. Fig. 4 shows the resulting block diagram for the motion controlled hexapod in operational space coordinates with state estimation.

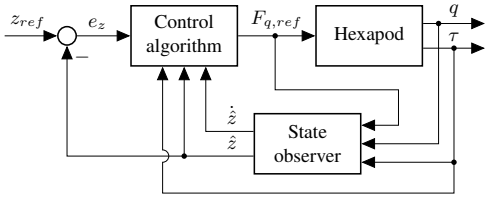

Fig. 4: Motion control of the hexapod in operational space coordinates with state estimation

A. Position control design

An inverse dynamics operational space position control law [18] can easily be obtained by rearranging the hexapod's equations of motion (1) for the actuator forces. This input transformation results in the feedback linearization

$$F_q = J^T(\hat{z}) \cdot \left(M(\hat{z}) \cdot u_{fl} + C(\hat{z}, \dot{\hat{z}}) \cdot \dot{\hat{z}} + g(\hat{z}) + \tau \right) \qquad (3)$$

with u_{fl} being the new control input. In (3), the actual values of z and $\dot{z}$ were replaced by their estimated counterparts.

In case of a perfect match of the controlled system and the corresponding system model used for feedback linearization as well as ideal state estimation, using (3) leads to an ideally decoupled system with double integral behavior for each DOF regarding u_{fl}, i.e.

$$\ddot{z} = u_{fl}.$$

Test rig measurements reinforce that these assumptions are not only valid for the simulation model but for the real system as well. The incorporation of the measured forces and torques τ in (3) renders the end effector infinitely stiff regarding external stress [18] as long as the control input limitations are respected.

With (3), the control input u_{fl} can now be chosen as

$$u_{fl} = \ddot{z}_{ref} + R_D \cdot \left(\dot{z}_{ref} - \dot{\hat{z}}\right) + R_P \cdot \left(z_{ref} - \hat{z}\right)$$

where $R_D, R_P \in \mathbb{R}^{6\times 6}$ are diagonal matrices. The implementation of the given equations on the target system realizes a decoupled PD position control of the hexapod's end effector platform. Under the assumptions made above, the system's position error dynamics is given by

$$\ddot{e}_z + R_D \cdot \dot{e}_z + R_P \cdot e_z = 0$$

with the generalized position error e_z. The comparison of this equation to a homogeneous second order differential equation with parameters ω (the angular frequency) and D (the damping ratio) leads to the equations

$$R_P = \omega^2 \qquad\qquad R_D = 2 \cdot D \cdot \omega$$

which provide an illustrative means for the dimensioning of R_P and R_D. The following values were used as a starting point for position control design: $\omega = 2 \cdot \pi \cdot 50$ and $D = 1/\sqrt{2}$. These values were supplemented by tuning factors for each DOF which were used to successively increase position control performance when the test rig was put into operation. Using this approach, a closed-loop position control bandwidth of about $60\,\mathrm{Hz}$ in vertical direction, $50\,\mathrm{Hz}$ in the planar directions and $30\,\mathrm{Hz}$ to $40\,\mathrm{Hz}$ in the rotational DOFs was achieved. Refer to [15] for a plot of the frequency response and a short excerpt of the time plot of the control performance in vertical direction for a rough-road maneuver.

B. Force control design

To control the force respectively the torque in particular directions rather than the position or angle, the given position control loop is superimposed by a force control loop. This concept is called direct force control with inner position control in the literature [18]. To enable the operator to freely choose between force and position control in each of the end effector's six DOFs, a hybrid position / force control framework was adopted on the test rig. The sequence of entries in the selection matrix S has to match the one found in the generalized position vector z, e.g.

$$S = \mathrm{diag}\left(\begin{bmatrix}1 & 1 & 0 & 1 & 0 & 1\end{bmatrix}\right) \tag{4}$$

means that the forces F_x, F_y, the vertical position r_z, the torques M_x and M_z as well as the angle β (the angle around y resembling the wheel's rotation) are controlled to given desired values. S was chosen this way to realize position control in the unconstrained directions (β) and force control in the constrained directions. The only exception is the vertical degree of freedom r_z which is mostly used to reproduce given measured position references on our test rig and, thus, position control was chosen over force control. Fig. 5 shows the hybrid control structure implemented on the test rig which was adapted to a direct force control approach compared to the illustration found in [12].

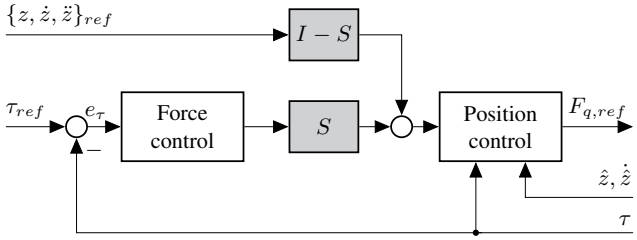

Fig. 5: Hybrid position / force control

Depending on the choice of the elements of S, a specific DOF is either controlled to a target position value ($s_i = 0$) or the force controller alters the current position target value to achieve a given target force value ($s_i = 1$). Naturally, as for other approaches, it is generally not possible to control both force and position to a desired value. However, it is possible to use the position reference value path for feedforward purposes in case of a force controlled DOF, cf. [19].

As outlined in [18], an integral action is required for the force controller so that the desired value is reached at steady state. Thus, a proportional-integral-derivative (PID) force controller was chosen for the target system. Due to the high complexity of the overall plant including the hexapod, the axle and the wheel force transducer, finding parameters for this controller is not a trivial task. Fortunately, it turned out that, as for the position controller, the six force controllers can be designed relatively independent of each other.

In order to put the controller in operation, a detailed multibody simulation model of the axle test rig was used to obtain reliable, initial values for the controllers' parameters. By using the chosen values in simulations, desired force respectively torque values were attained moderately fast without an overshoot for each direction.

For the purpose of control design, a square force respectively torque reference value was provided to the controller. Its parameters were then successively changed until a satisfying control performance was achieved. This procedure was carried out while specific code on the real-time hardware permanently monitored the system, providing a foolproof environment for control design. Most importantly, it reset the controller values to the last known, stable configuration given the slightest indication of unstable system behavior. Given this framework, the initial commission of these controllers was successful and control performance was successively increased experimentally on the test rig.

V. Validation on the Test Rig

This section provides an impression of the achieved force control performance by showing measurements obtained during actual test rig experiments. The measurements were carried out with the controller configuration given by (4).

During the first experiment, the hexapod performs a series of square-wave force pulses in lateral direction (F_y, max. peak to peak value $2\,\mathrm{kN}$) followed by a series of square-wave position pulses in vertical direction (z, max. peak to peak value $4\,\mathrm{mm}$) within a total time of $0.6\,\mathrm{s}$. Throughout this measurement, the desired values are subject to second-order low-pass filtering ($f = 40\,\mathrm{Hz}$, $D = 1$). Fig. 6 illustrates the result of this experiment.

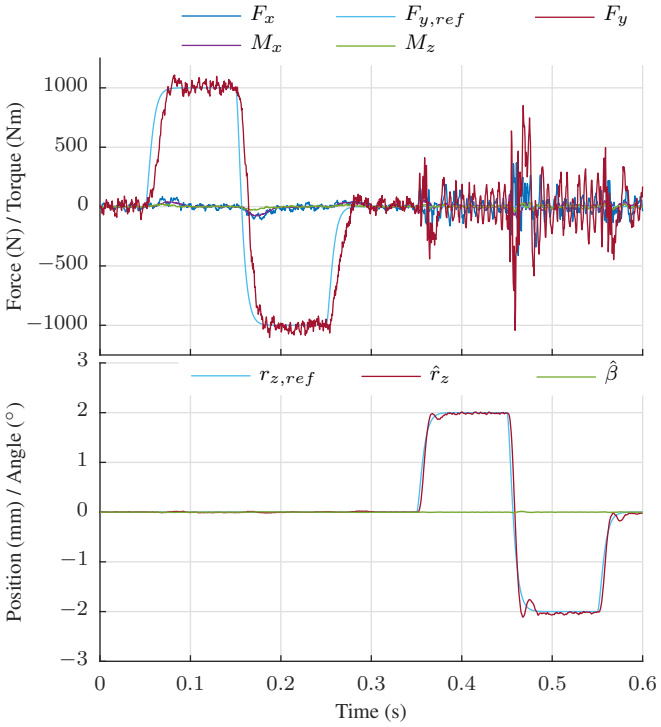

Fig. 6: Test rig measurement for a force square in lateral direction followed by a position square in vertical direction

In this figure, the upper plot compares the desired lateral force $F_{y,ref}$ and its actual value F_y. It also shows the resulting forces and torques in the other force-controlled DOFs which have a constant reference value of $0\,\mathrm{N}$ respectively $0\,\mathrm{Nm}$ not depicted in the figure. The lower plot shows the corresponding values for the position-controlled DOFs. They are given in terms of the relative deviation with respect to a specified operating point. Again, as a constant reference value for the rotation around axis y of $0°$ was chosen, only the estimated value of the angle β is shown. For the vertical position r_z both the desired and estimated value are depicted.

While the control approach outlined above achieves a considerably good decoupling regarding the positions / angles on the test rig, this is naturally not the case for the forces / torques. On force level, the DOFs remain cross-coupled as this effect was not accounted for during control design. Thus, an excitation in a specific direction impacts the other directions as well.

However, the first half of the experiment shows that the force controllers in the other directions can cope with the high force changes in lateral direction as the corresponding forces and torques remain rather low. Furthermore, as evident from the lower plot, this excitation has no significant impact on the position-controlled DOFs r_z and β. Regarding F_y, a good and fast tracking of the reference value can be observed. In this direction, the signal noise is higher by a factor of three or more compared to the other DOFs due to the underlying measurement principle.

The second half of the experiment shows the high bandwidth of the position controller. It also shows that the force controllers cannot keep the resulting forces and torques at $0\,\mathrm{N}$ respectively $0\,\mathrm{Nm}$ given the vertical position square excitation as good as for the force excitation. The highest force peaks arise for F_y.

There are, at least, two obvious reasons for this. Firstly, as obtained from other measurements, the stiffness in y-direction is very high ($c_y \approx 5000\,\mathrm{N\,mm^{-1}}$) when compared to the other directions (e.g. $c_x \approx 390\,\mathrm{N\,mm^{-1}}$). As the ideal wheel trajectory is not a perfect straight in vertical direction, a sole vertical excitation violates the ideal trajectory and results in lateral forces and torques which have to be compensated for by the corresponding controllers. Given the high stiffness c_y, these small deviations from the ideal curve implicate high forces F_y. Secondly, the position controller is fastest in vertical direction. Due to the chosen direct force control approach with subordinate position controller, the force controller's bandwidth is limited by the bandwidth of the position controller. Hence, no force controller can be expected to ideally compensate for the impacts of the r_z-controller.

All in all, the force control performance is quite good. Still, the experiment exhibits potential improvements such as the reduction of the cross-couplings on force level.

In contrast to the previous plot, Fig. 7 actually shows the result of four experiments. They have in common that the axle is exposed to a desired sinusoidal lateral force $F_{y,ref}$ of magnitude $1\,\mathrm{kN}$. The frequency is successively increased by $10\,\mathrm{Hz}$ starting at $10\,\mathrm{Hz}$. To keep the time range unchanged, an additional full wave is added for each consecutive plot. Regarding the other DOFs, the desired values are constantly held at 0. The signals and their respective colors are identical to those found in the upper plot in Fig. 6. Here, r_z and β are not shown as the deviations in these directions are barely noticeable for the given experiments.

First of all, the impact of the sinusoidal force F_y on the other force-controlled DOFs is very low for all four experiments. Apart from that, Fig. 7 provides a good means to assess force control bandwidth in lateral direction. The magnitude of F_y decreases when the excitation frequency rises. Even for $40\,\mathrm{Hz}$, it still amounts to approximately $70\,\%$ ($-3\,\mathrm{dB}$) of the excitation magnitude $1\,\mathrm{kN}$. Additionally, a nearly constant time shift between desired and measured force value is evident. This indicates an almost linear relationship between excitation frequency and phase shift. The phase shift amounts to roughly 29, 43, 60 and $75°$ for 10, 20, 30 and $40\mathrm{Hz}$.

It has to be noted that the nonlinear system behavior depends on the given excitation. Hence, control performance might be better or worse for other excitations. However, the

presented force controller with constant parameters appears to be quite robust.

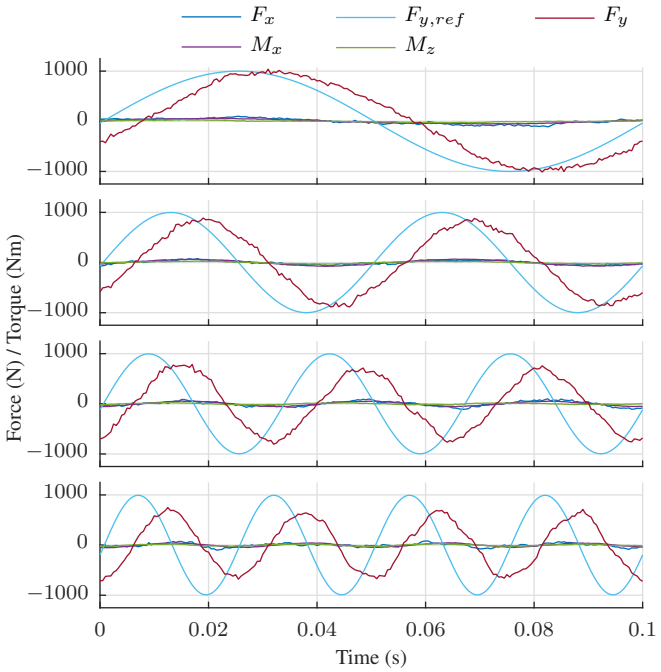

Fig. 7: Test rig measurement for a force sinusoidal in lateral direction (Magnitude 1 kN, frequencies 10, 20, 30 and 40 Hz from top to bottom)

VI. Conclusion

This contribution presented the hybrid position / force control strategy to operate a hydraulically actuated hexapod which serves as an excitation unit in HiL axle tests. An emphasis was put to the assessment of the force control performance achieved with the given control setup. Actual test rig measurements proved the general functionality of the approach and demonstrated an already high performance of the force controllers. They also identified potential improvements and pointed the way for upcoming research.

Regarding control design, future work will focus on the derivation of force feed forward control approaches and suitable countermeasures for the cross-coupling on force level. Furthermore, the manual control dimensioning process is intended to be replaced by an optimization. Due to the obvious limitation of the achievable force control bandwidth with the given approach, other force control approaches such as direct force control with subordinate velocity control and explicit force control will be tested on the system. Additionally, a lot of effort is put into the derivation of the overall system's model including hexapod and axle as well as the completion of the HiL environment.

Acknowledgment

The development and setup of the HiL axle test rig was funded by the Deutsche Forschungsgemeinschaft's (DFG) Major Research Instrumentation Programme.

References

[1] R. M. Schupbach and J. C. Balda, "A versatile laboratory test bench for developing powertrains of electric vehicles," in *2002 IEEE 56th Vehicular Technology Conference*, Vancouver, Canada, 2002, pp. 1666–1670.

[2] S. Oncu, S. Karaman, L. Guvenc, S. S. Ersolmaz, E. S. Ozturk, E. Cetin, and M. Sinal, "Robust yaw stability controller design for a light commercial vehicle using a hardware in the loop steering test rig," in *2007 IEEE Intelligent Vehicles Symposium*, Istanbul, Turkey, 2007, pp. 852–859.

[3] L. Heidrich, B. Shyrokau, D. Savitski, V. Ivanov, K. Augsburg, and D. Wang, "Hardware-in-the-loop test rig for integrated vehicle control systems," *IFAC Proceedings Volumes*, vol. 46, no. 21, pp. 683–688, 2013.

[4] A. Bouscayrol, "Different types of hardware-in-the-loop simulation for electric drives," in *2008 IEEE International Symposium on Industrial Electronics*, 2008, pp. 2146–2151.

[5] S. Flottmeier, K.-P. Jäker, and A. Trächtler, "Test rig for the hardware-in-the-loop simulation of mechatronic axles," in *Proceedings of the 9th International Fluid Power Conference*, vol. 3, Aachen, 2014, pp. 366–377.

[6] S. Olma, A. Kohlstedt, P. Traphöner, K.-P. Jäker, and A. Trächtler, "Substructuring and control strategies for hardware-in-the-loop simulations of multiaxial suspension test rigs," in *Proceedings of the 7th IFAC Symposium on Mechatronic Systems*, Loughborough, UK, 2016, pp. 141–148.

[7] ——, "Indirect force control in hardware-in-the-loop simulations for a vehicle axle test rig," in *14th International Conference on Control, Automation Robotics & Vision (ICARCV)*, Phuket, Thailand, 2016.

[8] F. Paccot, N. Andreff, and P. Martinet, "A review on the dynamic control of parallel kinematic machines: Theory and experiments," *The International Journal of Robotics Research*, vol. 28, no. 3, pp. 395–416, 2009.

[9] I. Davliakos and E. Papadopoulos, "Impedance model-based control for an electrohydraulic stewart platform," *European Journal of Control*, vol. 15, no. 5, pp. 560–577, 2009.

[10] *On the force-controlled assembly operations of a new parallel kinematics manipulator*, Rhodes, 2003.

[11] S. Bellakehal, N. Andreff, Y. Mezouar, and M. Tadjine, "Vision/force control of parallel robots," *Mechanism and Machine Theory*, vol. 46, no. 10, pp. 1376–1395, 2011.

[12] M. H. Raibert and J. J. Craig, "Hybrid position/force control of manipulators," *Journal of Dynamic Systems, Measurement, and Control*, vol. 103, no. 2, pp. 126–133, 1981.

[13] C. Holz, "Positions- und Kraftregelung eines linear direkt angetriebenen Hexapoden," Ph.D. dissertation, University of Hannover, Hannover, 2007.

[14] T. Muller and C. Endisch, "Compensation techniques for iterative rig control in multi-axial durability testing," in *2016 IEEE 21st International Conference on Emerging Technologies and Factory Automation (ETFA)*, 2016, pp. 1–7.

[15] A. Kohlstedt, S. Olma, S. Flottmeier, P. Traphöner, K.-P. Jäker, and A. Trächtler, "Control of a hydraulic hexapod for a hardware-in-the-loop axle test rig," *at - Automatisierungstechnik*, vol. 64, no. 5, 2016.

[16] S. Flottmeier, S. Olma, and A. Trächtler, "Sliding mode and continuous estimation techniques for the realization of advanced control strategies for parallel kinematics," *IFAC Proceedings Volumes*, vol. 47, no. 3, pp. 182–190, 2014.

[17] S. V. Drakunov and M. Reyhanoglu, "Hierarchical sliding mode observers for distributed parameter systems," *Journal of Vibration and Control*, vol. 17, no. 10, pp. 1441–1453, 2011.

[18] B. Siciliano, L. Sciavicco, L. Villani, and G. Oriolo, *Robotics: Modelling, planning and control*, ser. Advanced textbooks in control and signal processing. London: Springer, 2010.

[19] A. Kohlstedt, S. Olma, P. Traphöner, K.-P. Jäker, and A. Trächtler, "Kinematics-based force/position control of a hexapod in a hil axle test rig," in *Proceedings of the 17th Stuttgart International Symposium*, Stuttgart, 2017, pp. 1217–1230.